
Proceedings Paper:
Byers, R.A. orcid.org/0000-0001-8582-9325 and Matcher, S.J. (2019) Ghosting artifact reduction of polarization sensitive optical coherence tomography images through wavelet-FFT filtering. In: Fujimoto, J.G. and Izatt, J.A., (eds.) Proceedings of SPIE. Optical Coherence Tomography and Coherence Domain Optical Methods in Biomedicine XXIII, 02-07 Feb 2019, San Francisco, CA, USA. SPIE - Society of Photo-optical Instrumentation Engineers . ISBN 9781510623767

https://doi.org/10.1117/12.2511519

Ghosting artifact reduction of polarization sensitive optical coherence tomography images through wavelet-FFT filtering

Byers, R., Matcher, S.

R. A. Byers, S. J. Matcher, "Ghosting artifact reduction of polarization sensitive optical coherence tomography images through wavelet-FFT filtering," Proc. SPIE 10867, Optical Coherence Tomography and Coherence Domain Optical Methods in Biomedicine XXIII, 1086733 (22 February 2019); doi: 10.1117/12.2511519

SPIE.

Event: SPIE BiOS, 2019, San Francisco, California, United States

Ghosting Artefact Reduction of Polarization Sensitive Optical Coherence Tomography Images through Wavelet-FFT Filtering

R. A. Byers*[a], S. J. Matcher[b]
[a]Dept. of Infection & Immunity & Cardiovascular Disease, Univ. of Sheffield, Beech Hill Road, Sheffield, S10 2RX; [b]Dept. of Electronic and Electrical Engineering, Univ. of Sheffield, Broad Lane, Sheffield, S3 7HQ.

ABSTRACT

Undesirable cross-coupling between polarisation-maintaining (PM) fibers can result in detrimental ghost artefacts within polarisation sensitive optical coherence tomography (PS-OCT) images. Such artefacts combine with coherence noise stripes (originating from Fresnel reflections of optical components), complex-conjugate derived mirror-images and further irregular autocorrelation terms originating from the sample. Together, these artefacts can severely degrade the detected images, making quantitative measurements of the tissue birefringence challenging to perform.

In this work, we utilize the recently presented wavelet-FFT filter[1] to efficiently suppress these imaging artefacts entirely through post-processing. While the original algorithm was designed to suppress one-dimensional stripe artefacts, we extend this methodology to also facilitate removal of artefacts following a duplicate or inverse (mirror) profile to that of the skin surface. This process does not require any hardware modification of the system and can be applied retroactively to previously acquired OCT images.

The performance of this methodology is evaluated by processing artefact-corrupted PS-OCT images of skin consisting of simultaneously detected horizontal and vertical polarized light. The resulting images are used to calculate a phase retardance map within the skin, the profile of which is indicative of localized birefringence. Artefacts in the resulting processed PSOCT images were notably attenuated compared to the unprocessed raw-data, with minimal degradation to the underlying phase retardation information. This should improve the reliability of curve-fitting for measurements of depth-resolved birefringence.

Keywords: Polarization Sensitive, Optical Coherence Tomography, Image Artefacts, Ghost Artefacts, Wavelet-FFT filtering, Image Processing.

1. INTRODUCTION

Polarization sensitive optical coherence tomography (PS-OCT) is a non-invasive optical modality which utilizes the polarimetric information carried within transverse light waves to infer measurements of the polarization properties within a sample. PS-OCT has been used extensively within biological tissues, finding particular application in opthalmology[2], dermatology[3], dentistry[4] and for the enhanced study of tendon, bone, cartilage and ligaments[5]. Recently, PS-OCT systems comprised of polarization-maintaining (PM) fibers have been developed[6–9], which are more clinically applicable and less prone to systematic errors when compared to systems utilizing bulk optics[10]. Such systems also avoid the undesirable polarization state fluctuations during beam propagation along single-mode (SM) fibers[6,11]. One notable disadvantage of PM fiber based systems is the introduction of ghost-image artefacts, which arise due to refractive index differences between the two orthogonal polarization modes of the fiber, effectively slowing beam propagation along one axis of the elliptic fiber core with respect to the other[6]. Imperfections in splice angles and at fiber connectors can result in undesirable cross-coupling between the two channels[6,7], creating vertically offset copies of the image which limit the accuracy of corresponding birefringence measurements. A hardware based method of removing these artefacts involves displacing them out of the OCT imaging range through the use of long PM fiber segments[7].

*r.byers@sheffield.ac.uk; Tel: +44 (0)114 21 59539; http://www.sheffield.ac.uk/iicd/dermatology

Optical Coherence Tomography and Coherence Domain Optical Methods in Biomedicine XXIII
edited by James G. Fujimoto, Joseph A. Izatt, Proc. of SPIE Vol. 10867, 1086733
 · doi: 10.1117/12.2511519

In cases where precise implementation or hardware based compensation is not practical, we propose that a post-processing algorithm may improve visualization of the depth-resolved phase retardance profile. For this, the recently presented wavelet-FFT filter[1] is utilized.

2. METHODOLOGY

2.1 PS-OCT system

To evaluate the efficacy of the algorithm, multiple PS-OCT images were acquired from a healthy volunteer (27 years old, Fitzpatrick skin type III) at various skin sites. The PM-fiber based PSOCT system which was used follows the scheme reported by Al-Quasi *et al*[7] and is detailed fully in a previous publication[9], the system layout is illustrated in Fig. 1 below. Briefly, a Panda PM-fiber Mach-Zehnder interferometer directs circularly polarized light to the sample, where internal structures modify the polarization state of the backscattered light. The horizontal and vertically polarized signals are then detected separately by two balanced detectors (1817-FC, New Focus, US) and used to calculate the phase retardance profile within the tissue, without the requirement for auxiliary optical components. The light source used was a commercially available swept-source laser (HSL-2000-10-MDL, Santec Japan) which has a center wavelength of 1315nm, a sweep range of 157nm and a full width at half maximum (FWHM) of 128nm. The measured resolution (in-air) of the system was approximately 10μm and the laser was set to sweep at a rate of 10 kHz.

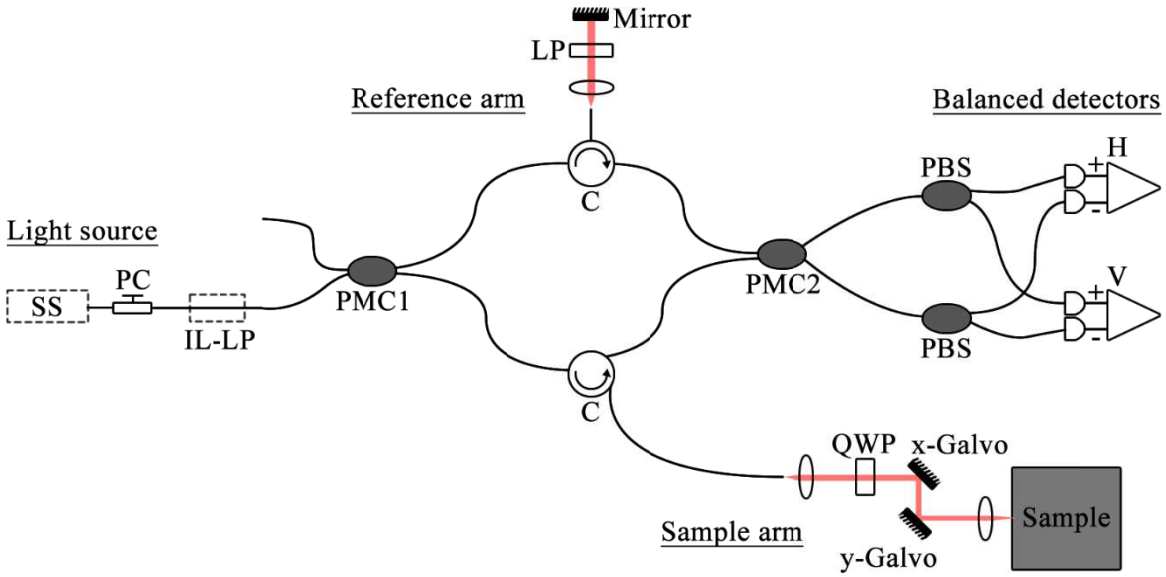

Figure 1. Schematic diagram of the PM-fiber based PSOCT system. SS: Swept-source light source, PC: polarization controller, IL-LP: in-line linear polarizer, PMC1/2: polarization-maintaining couplers, QWP: quarter waveplate, PBS: polarization beamsplitter, H/V: Balanced photo-detectors which detect the horizontal and vertically polarized light.

2.2 Wavelet-FFT filtering

Wavelet-FFT filtering[1] falls under a subset of destriping image processing algorithms which aim to suppress line or "stripe" artefacts within an image. Uniform horizontal stripes have high frequency components in the vertical direction, thus a basic implementation of a destriping algorithm may simply attenuate the frequencies along the vertical ($u_x = 0$) axis of the 2D FFT $F(u_x, u_y)$ of an image $f(x, y)$, while maintaining the offset coefficients at $u_y = 0$. Münch *et al* demonstrated that by first wavelet filtering the image, such that the detail, diagonal, vertical and horizontal components of an image are reversibly condensed into separate bands, FFT filtering can be performed only on the relevant artifact corrupted band, improving preservation of the underlying image information when compared to the purely FFT based method[1].

The wavelet-FFT filter itself contains three variables which influence how effectively artefacts are suppressed:

1. The decomposition level (l) is the number of successive detail bands which are wavelet filtered.
2. Sigma (σ) defines the width of FFT coefficients which are damped within each horizontal band.
3. The type of wavelet used (e.g Haar, Daubechies 2, Daubechies 20).

For this work, the wavelet-FFT filter was configured to use: $l = 4$ and $\sigma = 10$ with a Daubechies 20 wavelet. These parameters were selected empirically, providing good results across a range of PS-OCT datasets, although improved results could potentially be obtained through optimization of the filter parameters.

2.3 Processing of PS-OCT images

Here, the combined wavelet-FFT filtering technique is expanded upon in order to facilitate the removal of multiple artefacts simultaneously, the entire process is summarized in Fig. 4. Firstly, the PS-OCT images derived from both the horizontal and vertically polarized channels are wavelet-FFT filtered to remove horizontal coherence noise stripes (Originating from Fresnel reflections from optical components). An assumption is made that the skin surface is unlikely to be flat, instead consisting of numerous bumps and ridges together with a general surface curvature. The attenuation of such stripes improves the image clarity and reduces anomalous detection of the horizontal stripes as the skin surface in the following step. The first application of the wavelet-FFT filter is illustrated in Fig. 2 below.

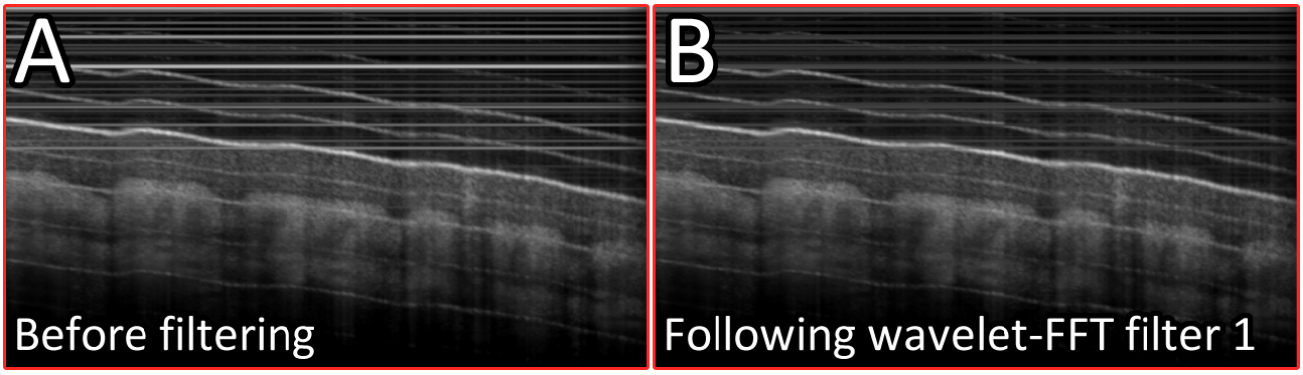

Figure 2. A) Unfiltered PS-OCT B-scan of the palm (Horizontal channel). B) The same B-scan as in A, following the first application of the wavelet-FFT filter. The same filtering process is also applied to the vertical channel.

The next step involved the detection of the skin-surface profile, this is made challenging due to the presence of the ghost artefacts. One previously utilized method of finding the skin surface involved finding the maximum in the signal gradient along each axial-scan[12], this method had a tendency to erroneously detect the artefacts as the skin surface as they often exhibit a similar signal gradient to that of the true skin surface, causing "jumps" in the surface profile. To address this, a path-finding optimization algorithm similar to that detailed previously[13] is employed. Firstly the assumption is made that the true skin surface is likely (But not guaranteed) to exhibit the highest signal intensities within the scan, thus a rough estimate of the skin surface location is found by identifying the location of the maxima along each axial-scan. Secondly, any "jumps" in this detected layer are removed as such changes in surface height are likely a result of the detection incorrectly identifying a ghost artefact as the true surface (A "jump" being defined as an axial difference between neighboring detections of greater than 5-pixels). Any gaps in the resulting detection are filled in using a connectivity-enforcing path-finding algorithm, which moves laterally across the detected surface and upon encountering a gap identifies the maximum value of only the 5-neighboring connected pixels. This is illustrated in Fig. 3 below.

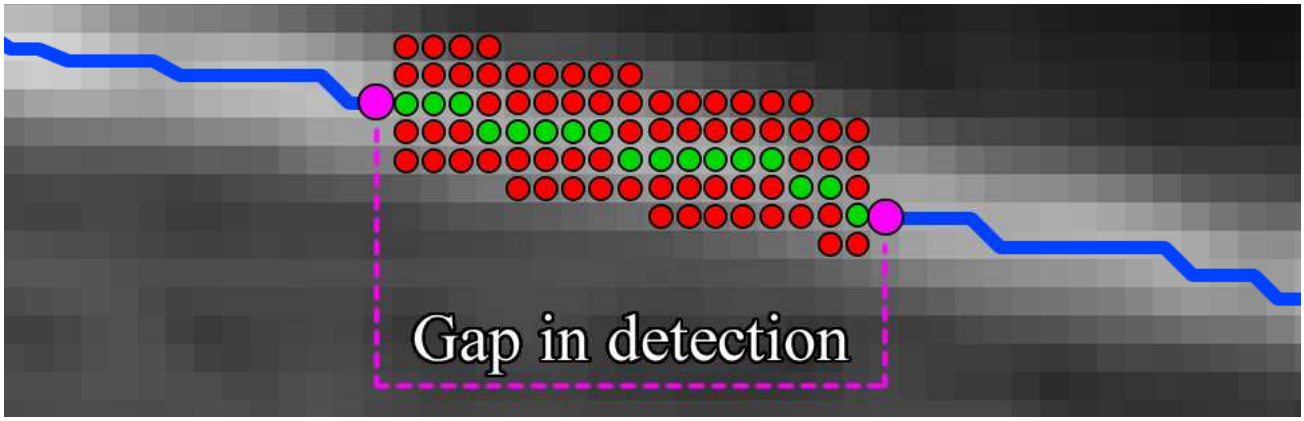

Figure 3. Zoomed view of a gap in the skin surface detection. Blue lines: Local maxima detection of the skin surface. Purple dashed line: A gap that had been removed due to a large >5 pixel "jump" in the signal. Green circles: Pixels which have been selected by the connectivity-enforcing path-finding algorithm and which now form part of the complete surface profile. Red circles: Pixels which have been considered, but rejected by the connectivity-enforcing path-finding algorithm.

Once the surface profile was found, displacement fields D (which flattened the skin surface and any ghost artefacts) and D^{-1} (The inverse transformation of D) were generated. To remove complex-conjugate derived "mirror-artefacts" which arise from structural or ghosting signal above the zero optical-path-difference (OPD) point of the system, the inverse surface transform D^{-1} was first applied (Flattening mirror artefacts), with wavelet-FFT filtering being applied a second time to remove them. The displacement field D was then applied twice, firstly to revert the displacement D^{-1} and a second time to flatten the skin surface and any associated ghosting artefacts. The skin surface$\pm$5-pixels was stored and wavelet-FFT filtering was applied a final time, removing the now horizontal surfaces from the image. The true stratum corneum, which was also removed during the final filtering process, could then be re-added to the image using the previously stored data, and any remaining autocorrelation related noise above the surface could simply be deleted by setting any pixels above the skin surface depth to zero. Fig. 4 summarizes the entire process.

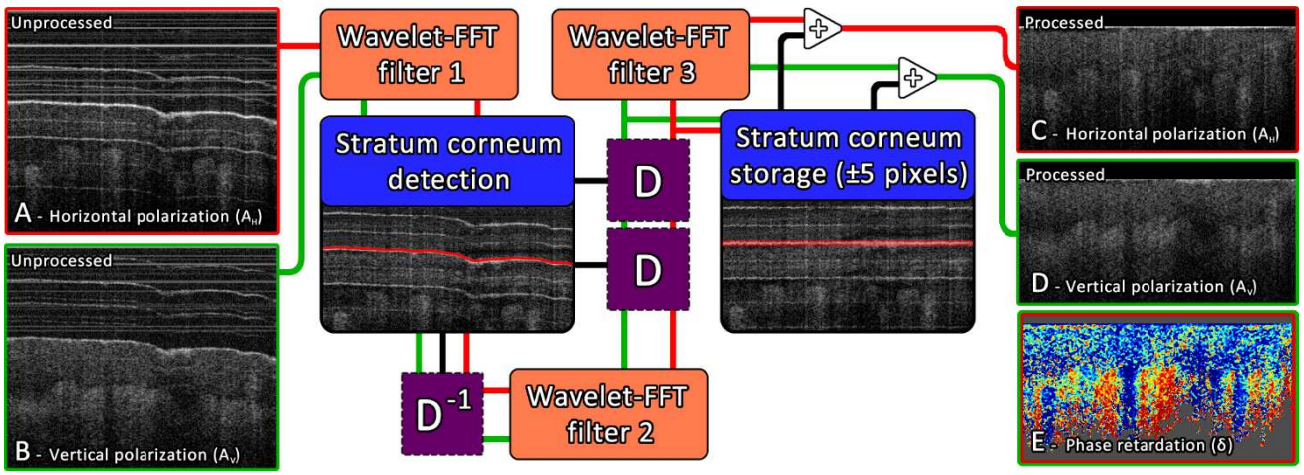

Figure 4. The proposed algorithm. A/B) Unprocessed horizontal/vertically polarized bscan. C/D) Processed horizontal/vertically polarized bscan. E) Phase retardance image: $\delta = \tan^{-1}(A_V/A_H)$. Scan captured from the palm.

3. RESULTS

Fig. 5 and Fig. 6 show the result of processing two different PS-OCT scans of the hand with the proposed algorithm.

Within the unprocessed reflectivity PS-OCT images of both the palm (Fig. 5A) and the dorsal hand (Fig. 6A), bright horizontal coherence lines and ghosting artefacts are visible both inside the sample and above the skin surface. Such lines increase the difficulty of reliable stratum corneum segmentation and corrupt both the B-scan image and the resulting phase retardance profiles (Fig. 5C and Fig. 6C). To compare within the tissue only, the unprocessed retardance images were masked using the same mask as used for the processed retardance images, setting background pixels to a gray coloration. The mask was generated as: $R_{Processed}(x, y) > 10$.

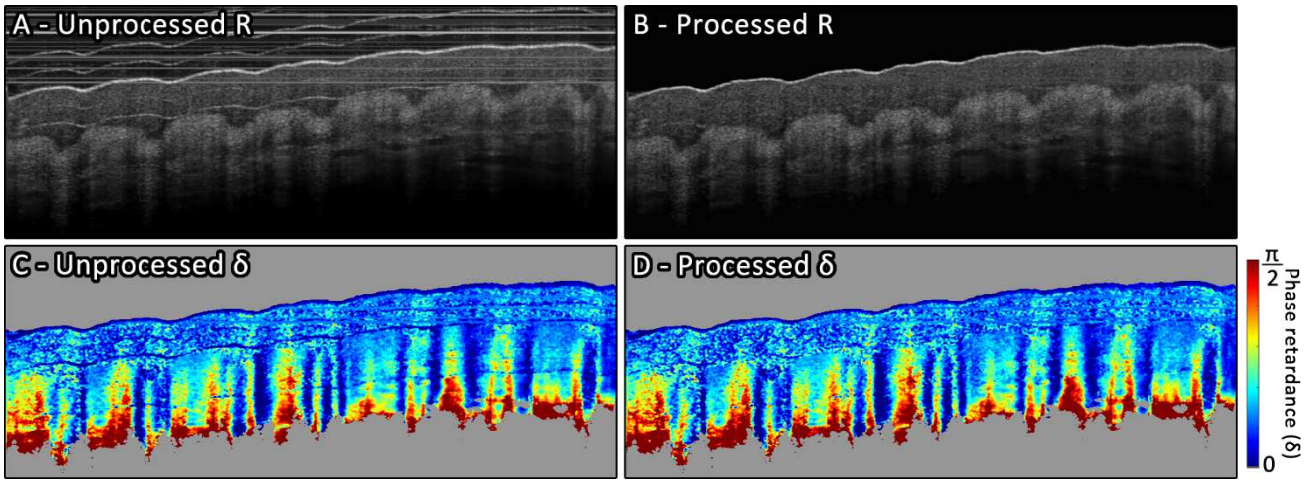

Figure 5. Results of processing a PS-OCT scan of the palm with the proposed algorithm. A) Unprocessed sample reflectivity image. B) Processed sample reflectivity image. C) Unprocessed phase retardance image. D) Processed phase retardance image. Reflectivity calculated as: $R = A_H^2 + A_V^2$, phase retardance calculated as: $\delta = \tan^{-1}(A_V / A_H)$. Where A_H and A_V are the amplitudes of the horizontal and vertically polarized PS-OCT signal respectively. To enable fair comparison of subsurface changes, a mask was generated from image B (R>10) and applied to both C and D.

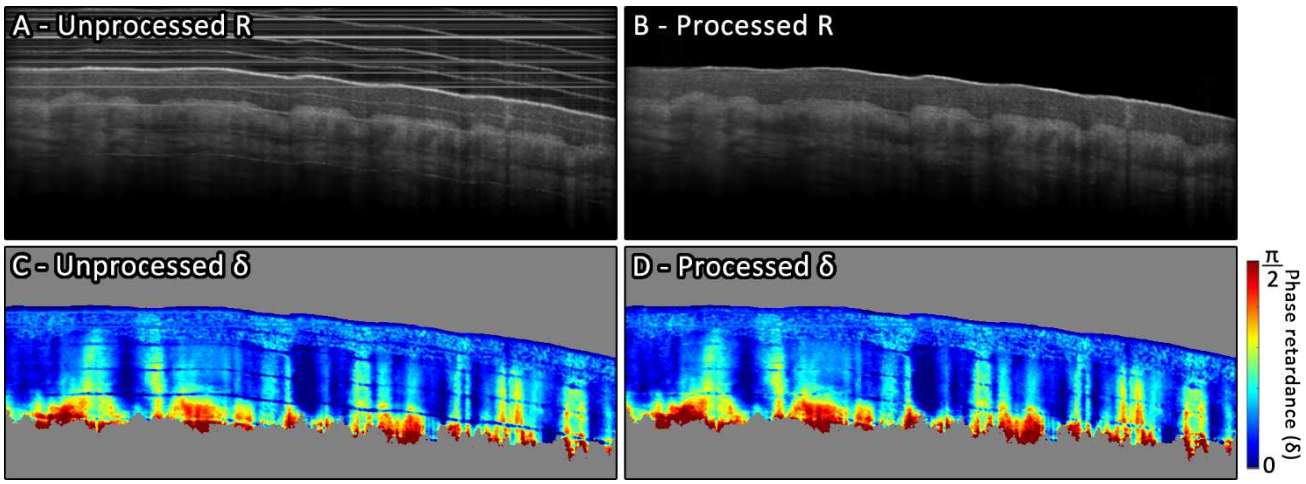

Figure 6. Results of processing a PS-OCT scan of the dorsal hand with the proposed algorithm. A) Unprocessed sample reflectivity image. B) Processed sample reflectivity image. C) Unprocessed phase retardance image. D) Processed phase retardance image. All images were calculated using the same method as in Fig. 5.

Following processing, the reflectivity images of both the palm (Fig. 5B) and the dorsal hand (Fig. 6B) have visibly fewer artefacts present, resulting in an improved visualization of the underlying tissue structure. Within the upper stratum corneum at both skin sites, faint horizontal lines have persisted through the processing. These are what remain of the horizontal coherence noise stripes, which (as shown on Fig. 2B) are heavily attenuated albeit not entirely removed following the first application of the Wavelet-FFT filter. In addition, small sections of the ghost copies of the skin surface have persisted, perhaps due to them not aligning in a perfectly flat manner following the skin surface flattening operation, resulting in non-uniform offset parameters in the frequency-domain. This is particularly noticeable on Fig. 6D, where the imprint of the ghost artefacts can still be seen (again heavily attenuated compared to the unprocessed scan) within the phase retardance profile of the dermis. It is possible that these remaining artefacts could be increasingly suppressed with further optimization of the wavelet-FFT filter parameters discussed in Sec. 2.2, however it is likely that the ideal choice of parameters will depend on how far the various stripes differ from ideal horizontal lines. For example, increasingly wide line artefacts can be more effectively removed by increasing the decomposition level (l) of the filter at the expense of some degree of image information. A more efficient approach in terms of preserving the underlying image information, particularly for blurred lines such as those observed here, may be to specifically FFT filter the decomposition levels which correspond to the range of stripe widths within the image[1].

4. CONCLUSIONS

In summary, this algorithm provides a simple method of reducing parasitic optical artefacts from PS-OCT images, and can be applied retroactively to previously acquired scans without any hardware modification to the OCT system. The resulting PS-OCT images contain visibly reduced coherence banding, together with a reduction in ghost/mirror artefact intensity, with no apparent degradation to the underlying image. This facilitates a clearer view of the depth-resolved phase retardance profile which could increase the reliability of curve-fitting methods for measurements of tissue birefringence. Future work could focus on the optimization of the filter parameters for specific datasets, allowing for more complete filtering of any present artefacts.

REFERENCES

[1] Münch, B., Trtik, P., Marone, F., and Stampanoni, M., "Stripe and ring artifact removal with combined wavelet--Fourier filtering.," Optics express 17(10), 8567–91 (2009).

[2] Pircher, M., Hitzenberger, C.K., and Schmidt-Erfurth, U., "Polarization sensitive optical coherence tomography in the human eye," Progress in Retinal and Eye Research 30(6), 431–451 (2011).

[3] Pierce, M.C., Strasswimmer, J., Park, B.H., Cense, B., and De Boer, J.F., "Advances in Optical Coherence Tomography Imaging for Dermatology" (2004).

[4] Walther, J., Golde, J., Kirsten, L., Tetschke, F., Hempel, F., Rosenauer, T., Hannig, C., and Koch, E., "In vivo imaging of human oral hard and soft tissues by polarization-sensitive optical coherence tomography," Journal of Biomedical Optics 22(12), 1 (2017).

[5] Baumann, B., "Polarization Sensitive Optical Coherence Tomography: A Review of Technology and Applications," Applied Sciences 7(5), 474 (2017).

[6] Davé, D.P., Akkin, T., and Milner, T.E., "Polarization-maintaining fiber-based optical low-coherence reflectometer for characterization and ranging of birefringence.," Optics letters 28(19), 1775–7 (2003).

[7] Al-Qaisi, M.K., and Akkin, T., "Polarization-sensitive optical coherence tomography based on polarization-maintaining fibers and frequency multiplexing," Optics Express 16(17), 13032 (2008).

[8] Götzinger, E., Baumann, B., Pircher, M., and Hitzenberger, C.K., "Polarization maintaining fiber based ultra-high resolution spectral domain polarization sensitive optical coherence tomography.," Opt. Express 17(25), 22704–22717 (2009).

[9] Kasaragod, D., Matcher, S.J., and Lu, Z., "Conical scan polarization-sensitive optical coherence tomography," Biomedical Optics Express, Vol. 5, Issue 3, pp. 752-762 5(3), 752–762 (2014).

[10] Schoenenberger, K., Colston, B.W., Maitland, D.J., Da Silva, L.B., and Everett, M.J., "Mapping of birefringence and thermal damage in tissue by use of polarization-sensitive optical coherence tomography," Applied Optics 37(25), 6026 (1998).

[11] Baumann, B., Hitzenberger, C.K., Pircher, M., Haindl, R., Zotter, S., Torzicky, T., and Trasischker, W., "Single

input state polarization sensitive swept source optical coherence tomography based on an all single mode fiber interferometer," Biomedical Optics Express, Vol. 5, Issue 8, pp. 2798-2809 5(8), 2798–2809 (2014).
[12] Byers, R.A., Maiti, R., Danby, S.G., Pang, E.J., Mitchell, B., Carré, M.J., Lewis, R., Cork, M.J., and Matcher, S.J., "Sub-clinical assessment of atopic dermatitis severity using angiographic optical coherence tomography," Biomedical Optics Express 9(4), 2001 (2018).
[13] Annan Li, Jun Cheng, Ai Ping Yow, Wall, C., Wong, D.W.K., Hong Liang Tey, and Jiang Liu, "Epidermal segmentation in high-definition optical coherence tomography," in 2015 37th Annu. Int. Conf. IEEE Eng. Med. Biol. Soc., 3045–3048 (2015).